

Spin waves in the nearly one-dimensional systems of CsNiCl_3 and RbNiCl_3

A. Sorgen

Department of Physics, Technion, Haifa, Israel

E. Cohen*

Bell Laboratories, Murray Hill, New Jersey 07974

J. Makovsky

Nuclear Research Center, Negev, P.O. Box 9001, Beer-Sheva, Israel

(Received 8 April 1974)

The magnetic excitations of CsNiCl_3 and RbNiCl_3 in their ordered state have been studied by optical absorption in the near infrared at $T = 1.7$ K. Magnon sidebands associated with the ${}^3A_{2g} \rightarrow {}^3T_{2g}$ excitons have been observed. The Hamiltonian of the spin system consists of intrachain (J_1) and interchain (J_3) interactions, both of the Heisenberg type with $J_1/J_3 \sim 40$ for CsNiCl_3 and ~ 20 for RbNiCl_3 , and a crystal-field single-ion anisotropy. The calculated equilibrium spin orientations agree with the "triangular configuration" observed by Yelon and Cox. Spin-wave theory is applied to calculate the magnon dispersion curves and density of magnon states. The large disparity between the intrachain and the interchain interactions results in the appearance of two sets of peaks in the calculated density of states. The high-energy set corresponds to magnons propagating along the chain, while the low-energy set corresponds to magnons propagating in the basal plane. This is in agreement with the observed single-magnon sidebands.

I. INTRODUCTION

In the research of low-dimensional magnetism, systems are often encountered in which a transition to a three-dimensional ordered state occurs at relatively low temperatures. In the case of nearly one-dimensional systems such a transition is induced by the weak coupling between chains of strongly coupled spins. An abundance of experimental data¹ indicate that, even in the three-dimensional ordered state, many properties are essentially characteristic of one-dimensional systems. Thus a linear dependence of the specific heat on temperature was observed^{2,3} well into the ordered state. The magnetic moment per spin at $T \rightarrow 0$ K (a quantity which assumes nonvanishing values only in the ordered state) has been found to be greatly reduced by zero-point motion.⁴⁻⁸ Such an effect is much more pronounced in one-dimensional systems than in two or three dimensions.^{9,10}

The ratio between intrachain and interchain interactions (denoted J_1/J_3 in this paper) is expected to determine the properties of a nearly one-dimensional system in both the paramagnetic and ordered states. The dependence of some static and dynamic properties on J_1/J_3 has been studied by Hennessy *et al.*¹¹ However, the dependence of the normal modes of the system on J_1/J_3 has not yet been investigated. In the celebrated case of the one-dimensional system of $(\text{CD}_3)_4\text{NMnCl}_3$, J_1/J_3 is probably of the order of 10^6 , and it has been shown¹² that spin-wave-like excitations can propagate along the chains even at fairly high tem-

peratures. These excitations have been found to follow a sinusoidal dispersion curve. The magnetic crystals of the $A\text{BCl}_3$ family¹³ (A —alkaline ion, B —transition-metal ion) as well as CsNiF_3 (Ref. 14) are known to exhibit one-dimensional characteristics. However, since they have Néel temperatures in the range of 2–10 K, the J_1/J_3 ratio is expected to be in range of 10–100. Some of these materials have single-ion anisotropy which is important in determining their magnetic properties.

In this paper we report the study of magnetic excitations of CsNiCl_3 and RbNiCl_3 in the limit of very low temperatures. Spin-wave theory is used to calculate the magnon dispersion curves and density of states. Since the intrachain exchange constant J_1 is almost identical for both crystals, while the interchain exchange constant J_3 is different, the dependence of magnon energies on the ratio J_1/J_3 can be studied. It is expected that the energies for magnons propagating along the chains will be the same for both crystals while the magnons propagating in the plane should have lower energies for smaller J_3 . The calculations are compared with observed magnon sidebands of the ${}^3A_{2g} \rightarrow {}^3T_{2g}$ excitons with good agreement between theory and experiment.

The paper is divided into two main parts. In Sec. II we describe the known magnetic properties of CsNiCl_3 and RbNiCl_3 and outline the experimental results. Section III contains the application of spin-wave theory to these crystals and a comparison between experiments and calculations. A short summary is given in Sec. IV.

II. MAGNETIC STRUCTURE AND EXPERIMENTAL RESULTS

A. Crystallographic and magnetic structures

CsNiCl_3 and RbNiCl_3 belong to a large group of transition-metal salts which have the space group D_{6h}^4 with two chemical units per unit cell.⁴⁻⁶ Figure 1(a) shows the unit cell of the paramagnetic phase in dotted line. The unit cell dimensions were determined by Achiwa¹³ and are $a_0 = 7.18$ (6.95) Å and $c_0 = 5.93$ (5.90) Å for CsNiCl_3 (RbNiCl_3). Figure 1(b) shows a projection of the unit cell on the basal plane (perpendicular to the c axis) with the two primitive hexagonal axes \vec{t}_1 and \vec{t}_2 .

Below T_N these crystals order antiferromagnetically, with a magnetic unit cell which is triple the size of the paramagnetic unit cell. $T_N = 11.1$ K for RbNiCl_3 (Ref. 5) while CsNiCl_3 has two transitions at 4.85 and 4.4 K.⁶ Below the second transition its magnetic structure is the same as that of RbNiCl_3 . The magnetic unit cell is shown in solid lines in Fig. 1(a). Its projection on the basal plane is shown in Fig. 1(b) with the hexagonal vectors \vec{t}'_1 and \vec{t}'_2 .

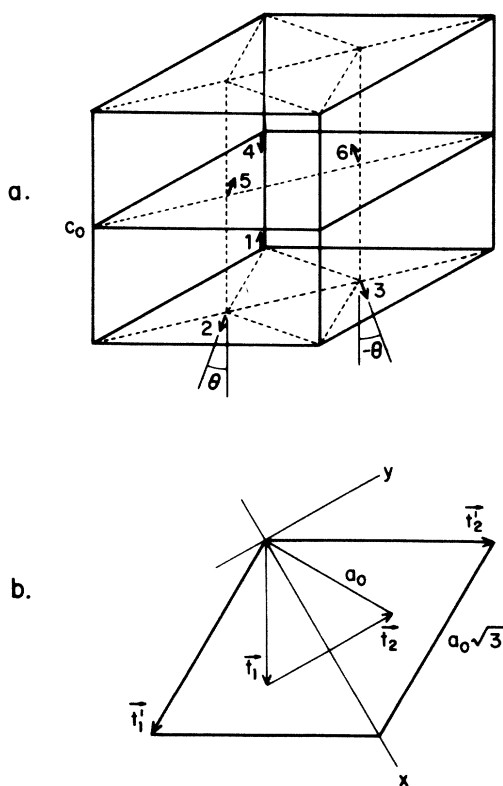


FIG. 1. (a) Chemical (dotted line) and magnetic (solid line) unit cells of CsNiCl_3 and RbNiCl_3 . The equilibrium orientation of the spins (in the absence of an external field) is shown schematically by arrows. (b) Projection of the unit cells on the basal plane.

If \vec{i} , \vec{j} , and \vec{k} denote unit vectors along the orthogonal axes x , y , and z ($c \parallel z$), then the two sets of primitive vectors are given by

$$\begin{aligned}\vec{t}_1 &= (a_0/2)(\sqrt{3}\vec{i} - \vec{j}), & \vec{t}'_1 &= (a_0\sqrt{3}/2)(\vec{i} - \sqrt{3}\vec{j}), \\ \vec{t}_2 &= a_0\vec{j}, & \vec{t}'_2 &= (a_0\sqrt{3}/2)(\vec{i} + \sqrt{3}\vec{j}), \\ \vec{t}_3 &= c_0\vec{k}, & \vec{t}'_3 &= c_0\vec{k}.\end{aligned}$$

The magnetic properties of CsNiCl_3 and RbNiCl_3 are expected to be determined mainly by the exchange interactions between three types of Ni^{2+} pairs.

(a) The nearest neighbors (nn) along the c axis. Each Ni^{2+} ion has two such nn ions at $\pm \frac{1}{2}c_0\vec{k}$.

(b) The next-nearest neighbors (nnn) along the c axis. Again there are two such nnn ions at $\pm c_0\vec{k}$.

(c) The next-next-nearest neighbors (nnnn) in the basal plane. Each Ni^{2+} ion has six such nnnn ions. They are conveniently grouped together in the two subgroups (i) the ions located at $-\vec{t}_1$, $-\vec{t}_2$, and $(\vec{t}_1 + \vec{t}_2)$ and (ii) those located at \vec{t}_1 , \vec{t}_2 and, $-(\vec{t}_1 + \vec{t}_2)$. The equilibrium spin orientation of the six sublattices was carefully studied by Yelon and Cox.^{5,6} They found that the nn spins in a given chain are oriented antiparallel to one another. This mutual orientation is preserved for temperatures well above T_N , owing to the relatively large intrachain exchange interaction¹³ J_1 . Within the basal plane (namely, the mutual orientation of the chains) the spins form a "triangular array" for $T < T_N$. This is shown schematically by the arrows numbered 1-6 in Fig. 1(a). The spins of one chain remain parallel to the c axis while the spins of the other two chains cant by an angle of $\pm \theta$ with respect to the c axis. In the case of CsNiCl_3 , the canting angle is found to depend on temperature, decreasing as $T \rightarrow 4.4$ K. Although other spin configurations were proposed, the model described here (numbered VI in Ref. 5 and I in Ref. 6) appears to be the most plausible since it is obtained by minimizing the classical expression for the energy per magnetic unit cell.

B. Crystal growth

CsNiCl_3 and RbNiCl_3 were prepared from an aqueous solution of equimolar quantities of CsCl or RbCl (Merck G. R.) and $\text{NiCl}_2 \cdot 6\text{H}_2\text{O}$ (Merck U. P.). The solution was solidified with hydrochloric acid, thoroughly mixed, and then boiled for a few minutes. The precipitate was washed with acetone and then dried in a vacuum desiccator at 140°C for 3 h. Single crystals were grown by the Bridgman technique in a vertical furnace. The temperature gradient at the freezing plane was about $25^\circ\text{C}/\text{cm}$ and the crystal was lowered at the rate of 1 mm/h. The resulting crystals were of good optical quality and possessed excellent cleav-

age planes containing the c axis.

C. Optical absorption studies

The optical spectrum of CsNiCl_3 and RbNiCl_3 in the visible and adjacent regions consists of broad absorption bands. Most of the bands are due to vibronic transitions but there are indications¹⁵ of ion-pair interaction contributing to the absorption intensity. Sharp lines are observed only for the ${}^3A_{2g} \rightarrow {}^3T_{2g}$ transition near $1.6 \mu\text{m}$. The absorption spectra in this region were taken on a 0.5-m Jarrell-Ash spectrometer equipped with a cooled PbS detector. The resolution of this spectrometer was better than 1 cm^{-1} . The crystals used were 1–4 mm thick and were cleaved in such a way that the light propagated in a direction perpendicular to

the c axis. Since it was difficult to cut and polish crystals with faces perpendicular to the c axis, most spectra were taken in σ and π polarizations. The quality of the spectra in α polarization was not sufficient for conclusive results. Typical spectra for both CsNiCl_3 and RbNiCl_3 , taken at 1.7 K, are shown in Fig. 2. Table I summarizes the transition wavelength and the frequency shift of the magnon sideband with respect to its parent transition.

As can be seen in Fig. 2, the σ and π spectra differ mainly in the absorption intensity and not in the spectral structure. The reason for this can be understood by considering the symmetry of the Ni^{2+} site in both paramagnetic and ordered phases. For $T > T_N$, each of the two Ni^{2+} ions in the unit cell has D_{3d} site symmetry. The ${}^3A_{2g}$

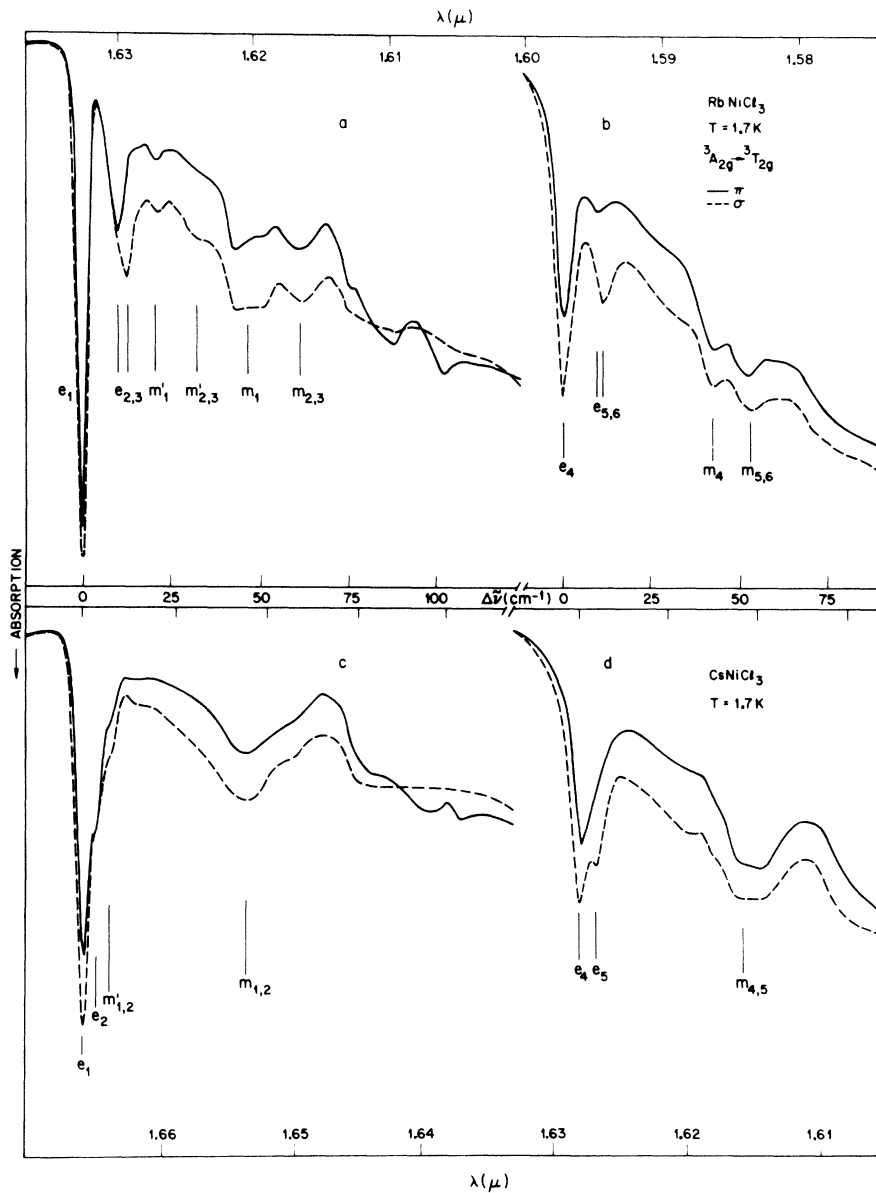


FIG. 2. ${}^3A_{2g} \rightarrow {}^3T_{2g}$ absorption spectra of RbNiCl_3 and CsNiCl_3 at 1.7 K. Only the sharp-line section is shown. e_i designate exciton transitions and m'_i and m_i the associated magnon sidebands. The gain in sections a and c is twice that of sections b and d.

TABLE I. Exciton transitions and magnon sidebands.

RbNiCl ₃			CsNiCl ₃		
Type	$\lambda(\mu\text{m})$	$\Delta\nu(\text{cm}^{-1})$	Type	$\lambda(\mu\text{m})$	$\Delta\nu(\text{cm}^{-1})$
e_1	1.6325		e_1	1.6657	
e_2	1.6297		e_2	1.6648	
e_3	1.6291				
$m'_{1,2}$	1.6269	21 : 1	$m'_{1,2}$	1.6636	8 : 1
$m'_{2,3}$	1.6240	20 : 1			
m_1	1.6200	46 : 3	$m_{1,2}$	1.6535	45 : 2
$m_{2,3}$	1.6167	47 : 2			
e_4	1.5963		e_4	1.6289	
$e_{5,6}$	1.5936		e_5	1.6277	
m_4	1.5850	45 : 2	$m_{4,5}$	1.6158	45 : 3
$m_{5,6}$	1.5820	49 : 2			

level splits into two states, A_{1g} and E_g , of D_{3d} . The ${}^3T_{2g}$ level is split by the trigonal-crystal-field and spin-orbit interaction into $A_{1g} + 2A_{2g} + 3E_g$ of D_{3d} . These single-ion states, when combined to give excitons with zero wave vector, will split into a multitude of states transforming like the irreducible representations of the D_{6h}^4 group at the point Γ . Only those excitons belonging to A_{2g} and E_g of Γ are allowed magnetic dipole transitions. If the ground-state splitting is small compared to kT , transitions will take place from both levels of ${}^3A_{2g}$. This will result in an unpolarized exciton spectrum in the paramagnetic phase, as is actually observed. For $T \ll T_N$, transitions occur only from the ground state of the ordered system. Thus, in principle, polarized spectra could be observed. However, the crystal symmetry is greatly reduced due to spin canting (the Ni^{2+} site symmetry is probably monoclinic⁵). This results in spectra which are virtually unpolarized. Therefore the assignment of the observed transitions is based mainly on two criteria: (a) the exciton transitions are sharper than the associated magnon sidebands, and (b) the frequency shift of the magnon sidebands is equal for all excitons and it agrees fairly well with the calculated magnon density of states.

A frequency-difference scale is given in the middle of Fig. 2. For each section the frequency shift is computed from the position of the lowest-energy exciton. It should be noted that in RbNiCl_3 the groups of excitons are well separated and so are the associated magnon sidebands. In CsNiCl_3 , however, the excitons are barely split, and thus the corresponding magnon sidebands merge. The bands shifted by 70 cm^{-1} or more are presumably two-magnon sidebands.

III. MODEL AND INTERPRETATION OF THE EXPERIMENTAL RESULTS

A. Spin Hamiltonian and equilibrium conditions

The magnetic properties of CsNiCl_3 and RbNiCl_3 are determined by the interactions between the

Ni^{2+} ions in the ${}^3A_{2g}$ state. Since the orbital momentum for this state is completely quenched, the exchange interactions are of the isotropic Heisenberg type. Because of the small trigonal distortion of the Ni^{2+} site symmetry, an axial crystal-line field provides the anisotropy term. With the designation of the six sublattices given in Fig. 1, the Hamiltonian has the form

$$\mathcal{H} = \sum_i D[(S_i^z)^2 - \frac{1}{3}S(S+1)] - 2J_1 \sum_{\langle i,4 \rangle} \vec{S}_i \vec{S}_j - 2J_2 \sum_{\langle i,1' \rangle} \vec{S}_i \vec{S}_j - 2J_3 \sum_{\langle i,2 \rangle} \vec{S}_i \vec{S}_j. \quad (1)$$

Here $S=1$, D is the axial crystalline field parameter for the ${}^3A_{2g}$ state, and the exchange constants between the various ion pairs are J_1 for nn ions, J_2 for nnn ions along the chain, and J_3 for nnnn ions on the same layer (interchain interaction).

In the ordered phase each spin is characterized by its equilibrium direction in space, which is here specified by the angles θ_i and ϕ_i . The Hamiltonian of Eq. (1) does not depend on the azimuthal angles ϕ_i . Such a dependence can be introduced by the Zeeman energy due to a field with a component in the basal plane.¹⁶ The classical energy per magnetic unit cell is then given by the following expression:

$$E_{\text{class}} = \sum_{m=1}^6 \left[\frac{1}{6} D(3 \cos^2 \theta_m - 1) - 2J_1 \cos(\theta_m - \theta_n) \right] - 3J_3 \sum_{i=1}^2 \left(\sum_{m=1}^3 \cos(\theta_m - \theta_{n'}) + \sum_{m=4}^6 \cos(\theta_m - \theta_{n''}) \right), \quad (2)$$

where $n = (m+3) \bmod 6$, $n' = (m+i) \bmod 3$, and $n'' = (m+i) \bmod 3 + 3$. The angles ϕ_i were fixed at $0, \pm \pi/2$ for the three nonequivalent sublattices in the basal plane. These values for ϕ_i fix all spins in the same plane in accordance with the structure determination.^{5,6}

Upon minimizing $E(\theta_1, \dots, \theta_6)$ the spin equilibrium directions are obtained. Assuming $|J_1| \gg |D|, |J_3|$, the nn spins align antiparallel to each other and this orientation is preserved even in the paramagnetic phase at sufficiently low temperatures. As for the interchain orientation, we have computed the values of θ_i which minimize E for various values of D and J_3 . When $D < 0$ we find that the spins on one chain remain parallel to the c axis while those on the two other chains cant at an angle of $\pi \pm \theta$ with respect to the c axis. In order to determine the dependence of θ on J_3 and D , we substitute $\theta_1 = 0, \theta_2 = \pi - \theta, \theta_3 = \pi + \theta$, and $\theta_n = \theta_m + \pi, n = m + 3$. Then

$$E(\theta) = 2D \cos^2 \theta - 12J_3(\cos 2\theta - 2\cos \theta) + 12J_1 \quad (3)$$

and $\min E(\theta)$ is obtained for

$$\theta = 0 \text{ for } 6|J_3| \leq |D|, \quad (4a)$$

$$\cos\theta = 6J_3/(12J_3 - D) \text{ for } 6|J_3| > |D|. \quad (4b)$$

The experimentally observed values for θ in the limit of very low temperatures are as follows: for RbNiCl₃, $\theta = 57.5^\circ$ (implying $J_3 = 1.2D$), and for CsNiCl₃, $\theta = 59^\circ$ (implying $J_3 = 2.8D$).

B. Spin waves

In order to obtain the spin-wave spectrum in the limit of very low temperatures, the Hamiltonian (1) has to be transformed into a bilinear form in the magnon creation and annihilation operators. However, a complication arises because of the canted spins: Walker's method¹⁷ cannot be directly applied since the crystal-field terms would be incorrectly transformed. Instead, we use a method which is a generalization of Grover's approach¹⁸ and is similar to that used by Allen.¹⁹

Using the mean field approximation, we calculate by a self-consistent algorithm the molecular field (both magnitude and direction) acting on each of the six sublattices. As expected, the equilibrium spin configuration obtained by this calculation (for a given set of J_1 , J_3 , and D) is identical with that obtained by minimizing the classical energy per spin. The calculation also provides a set of three "molecular-field states" ($S=1$) for each sublattice. These states span the subspace in which the magnetic excitations of the coupled-spin system are calculated. The Hamiltonian (1) is then projected onto the molecular-field subspace by the use of the method of projecting tensor operators.²⁰ The operators $a_m^\dagger(i)$ and $a_m(i)$ connect the ground and first excited states of the molecular-field subspace of the i th ion in the m th sublattice. By Fourier transforming these operators we obtain $a_{m,\vec{q}}^\dagger$ and $a_{m,\vec{q}}$, which are the creation and annihilation operators for single-spin excitation in the m th sublattice. In terms of these operators, the Fourier-transformed Hamiltonian will have the form

$$\mathcal{H}_{\text{SW}} = \sum_{\vec{q} \in \text{BZ}} \sum_{m,n=1}^3 (\alpha_{mn}(\vec{q}) a_{m,\vec{q}}^\dagger a_{n,\vec{q}} + \beta_{mn}(\vec{q}) a_{m,\vec{q}}^\dagger a_{n,-\vec{q}}^\dagger + \text{H. c.}) \quad (5)$$

$\alpha_{mn}(\vec{q})$ and $\beta_{mn}(\vec{q})$ depend on the interaction constants J_1 , J_2 , J_3 , and D and on the equilibrium orientation of each sublattice, namely, on θ_m . The form factors which are implicitly included in $\alpha_{mn}(\vec{q})$ and $\beta_{mn}(\vec{q})$ are given for each pair of sublattices:

$$f_{mn}(\vec{q}) = \cos \frac{1}{2} \vec{q} \cdot \vec{c}_0 \quad (6)$$

for intrachain pairs, and

$$f_{mn}(\vec{q}) = e^{i\vec{q} \cdot \vec{t}_1} + e^{i\vec{q} \cdot \vec{t}_2} + e^{-i\vec{q} \cdot (\vec{t}_1 + \vec{t}_2)} \quad (7)$$

for interchain pairs. Following White *et al.*,²¹ the summation over \vec{q} is restricted to the upper half of the Brillouin zone, and for each \vec{q} the Hamiltonian is written as a bilinear form

$$\mathcal{H}_{\text{SW}} = X^\dagger(\vec{q}) H(\vec{q}) X(\vec{q}), \quad (8)$$

with

$$X^\dagger(\vec{q}) = (a_{1\vec{q}}^\dagger, a_{1-\vec{q}}, \dots, a_{6\vec{q}}^\dagger, a_{6-\vec{q}}).$$

Since the operators satisfy boson commutation relations, the matrix $H(\vec{q})$ is non-Hermitian; it can be written as a product of two matrices:

$$H(\vec{q}) = g \cdot H'(\vec{q}). \quad (9)$$

$H'(\vec{q})$ is a Hermitian matrix with positive eigenvalues, and g is a diagonal matrix having alternating $+1$ and -1 along its diagonal. Brooks-Harris²² showed that such matrices have real eigenvalues, which occur in pairs $\pm \omega_s(\vec{q})$. The spin-wave energies are thus $\hbar \omega_s(\vec{q})$. In the present case $H(\vec{q})$ is a 12×12 matrix which is diagonalized numerically for each \vec{q} . The resulting spin-wave spectrum consists of six (generally nondegenerate) branches. A representative set of dispersion curves calculated for \vec{q} along high-symmetry directions in the Brillouin zone (BZ) is shown in Fig. 3. The density of magnon states was calculated using the linear extrapolation method²³ for a mesh of 605 points in the reduced BZ. The results obtained for two sets of interaction parameters are shown in Fig. 4. The parameters used in the calculations are (a) $J_1 = -10$, $J_2 = 0$, $J_3 = -0.6$, and $D = -0.5$ and (b) $J_1 = -10$, $J_2 = 0$, $J_3 = -0.3$, and $D = -0.15$ (all in units of cm^{-1}). As can be seen from Fig. 3, there is a much greater dispersion for magnons propagating along the chain than for those propagating in the basal plane. For magnons with $q_z = \pi/c$ the disper-

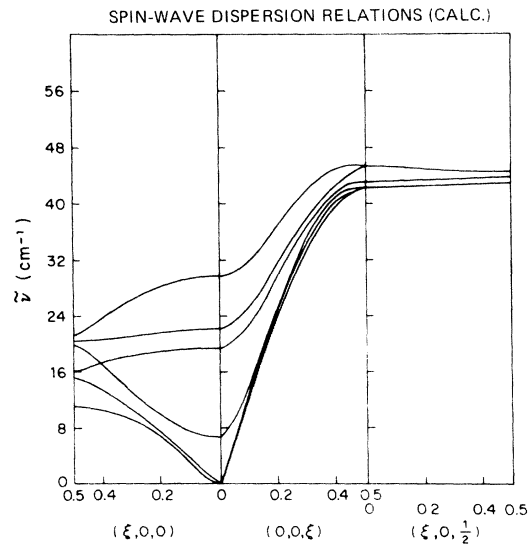


FIG. 3. Calculated spin-wave dispersion relations along some high-symmetry directions in the BZ. The parameters used are $J_1 = -10$, $J_2 = 0$, $J_3 = -0.6$, and $D = -0.5$ (all in units of cm^{-1}).

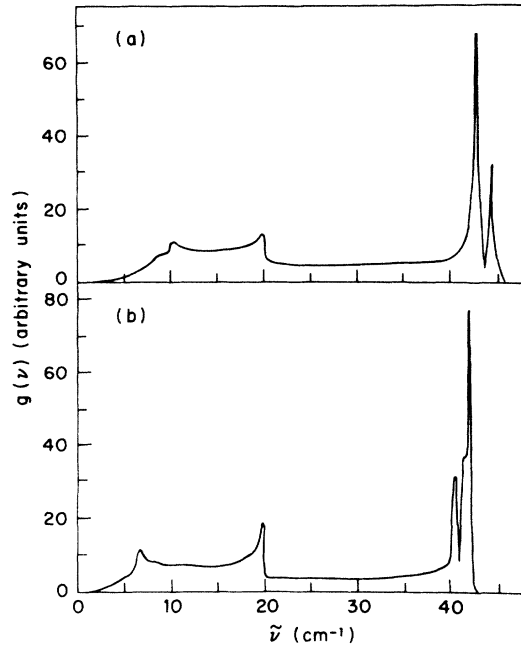


FIG. 4. Calculated density of magnon states for two sets of interaction parameters: (a) $J_1 = -10$, $J_2 = 0$, $J_3 = -0.6$, $D = -0.5$; (b) $J_1 = -10$, $J_2 = 0$, $J_3 = -0.3$, $D = -0.15$ (all in units of cm^{-1}).

sion curves are virtually flat. Consequently, the density of magnon states has peaks mainly around $\hbar\omega \sim 4J$. The smaller peaks in the lower-energy part correspond to magnons propagating in the basal plane. The energy of these magnon branches (in particular the "acoustic branches") depends on the value of J_3 (see Fig. 4).

Although there are no reliable exchange constants available (since no inelastic neutron scattering experiments were carried out on CsNiCl_3 and RbNiCl_3) they can be estimated fairly adequately from other

experimental data. From susceptibility measurements,^{7,13} J_1 is estimated to be of the order 9–11 cm^{-1} for both materials. This value will reproduce the position of the high-energy peaks in the magnon-sideband spectra ($\sim 45 \text{ cm}^{-1}$, designated m_i). It should be emphasized that no exciton-magnon interaction has been introduced in the calculation. This interaction can certainly shift the peak position in the spectrum and cause the broadening of observed peaks (cf. Figs. 2 and 4). The ratio J_1/J_3 can be estimated from its relation to the known T_N by using the calculation of Hennessy *et al.*¹¹ We then obtain $J_1/J_3 \sim 24$ for RbNiCl_3 and ~ 40 for CsNiCl_3 . However, we have used slightly smaller values in calculating the densities shown in Fig. 4. Even then the fit to the low-energy peaks (designated m'_i) is not as good as for the high-energy ones. Finally, the values for D are given by the equilibrium conditions (Sec. III A).

IV. SUMMARY

The relative contributions of both magnons propagating along the chain and those propagating in the basal plane to the magnon sidebands have been studied. Although the exciton-magnon interaction has not been taken into account, the single-magnon sideband can be understood by comparing it with the calculated density of magnon states. The largest contribution comes from magnons with $q_z = \pi/c$. These magnons persist as spin oscillations for temperatures higher than T_N , which is a manifestation of the one-dimensional character of CsNiCl_3 and RbNiCl_3 . It is thus of interest to investigate the temperature dependence of the magnon sidebands. This study is now under way.

ACKNOWLEDGMENTS

The authors wish to acknowledge many useful discussions with Dr. M. D. Sturge and Dr. L. R. Walker.

*On leave of absence from the Department of Physics, Technion, Haifa, Israel.

¹L. J. De Jongh and A. R. Miedma, *Adv. Phys.* **23**, 1 (1974). This review article contains many pertinent examples and references to experimental results.

²T. Haseda and A. R. Miedma, *Physica (Utr.)* **27**, 1102 (1961).

³M. Eibshütz, R. C. Sherwood, F. S. L. Hsu, and D. E. Cox, in *Proceedings of the 18th Annual Conference on Magnetism and Magnetic Materials*, Denver, 1972 (AIP, New York, 1973).

⁴D. E. Cox and V. J. Minkiewicz, *Phys. Rev. B* **4**, 2209 (1972).

⁵W. B. Yelon and D. E. Cox, *Phys. Rev. B* **6**, 204 (1972).

⁶W. B. Yelon and D. E. Cox, *Phys. Rev. B* **7**, 2024 (1973).

⁷P. A. Montano, E. Cohen, and H. Shechter, *Phys. Rev. B* **6**, 1053 (1972).

⁸G. R. Davidson, M. Eibshütz, D. E. Cox, and V. J.

Minkiewicz, in *Proceedings of the 17th Conference on Magnetism and Magnetic Materials*, Chicago, 1971, edited by C. D. Graham and J. J. Rhyne (AIP, New York, 1972).

⁹P. W. Anderson, *Phys. Rev.* **86**, 694 (1952).

¹⁰B. O. Loopstra, B. Van Laor, and D. J. Breed, *Phys. Lett. A* **26**, 526 (1968).

¹¹M. J. Hennessy, C. D. McElwee, and P. M. Richards, *Phys. Rev. B* **7**, 930 (1973). See also L. L. Liu and H. E. Stanley, *Phys. Rev. Lett.* **29**, 927 (1972).

¹²M. T. Hutchings, G. Shirane, R. J. Birgeneau, and S. L. Holt, *Phys. Rev. B* **5**, 1999 (1972).

¹³N. Achiwa, *J. Phys. Soc. Jap.* **27**, 561 (1969).

¹⁴M. Steiner, *Z. Angew. Phys.* **32**, 116 (1971).

¹⁵G. L. McPherson and G. D. Stucky, *J. Chem. Phys.* **57**, 3780 (1972).

¹⁶Basal-plane anisotropy can be important in the anti-ferromagnetic resonance (AFMR) of these materials, but since we are mainly interested here in $\vec{q} \neq 0$ magnons we neglect it. The AFMR of CsNiCl_3 and RbNiCl_3 will

- be dealt with in a subsequent publication.
- ¹⁷L. R. Walker, in *Magnetism*, edited by G. T. Rado and H. Suhl (Academic, New York, 1963), Vol. I.
- ¹⁸B. Grover, Phys. Rev. 140, A1944 (1965).
- ¹⁹S. J. Allen, Jr. and H. J. Guggenheim, Phys. Rev. B 4, 950 (1971).
- ²⁰P. Levy, J. Appl. Phys. 40, 1139 (1969). We have used the method of projecting tensor operators of any rank to calculate the magnetic excitations in systems with orbital angular momentum and in Heisenberg-type systems with canted spins. A full account will be presented elsewhere.
- ²¹R. M. White, M. Sparks, and L. Ortenburger, Phys. Rev. 139, A450 (1965).
- ²²A. Brooks-Harris, Phys. Rev. 132, 2398 (1963).
- ²³G. Gilat and L. J. Raubenheimer, Phys. Rev. 144, 390 (1966); 157, 586 (1967).